ELSEVIER
Available online at www.sciencedirect.com
ScienceDirect
Procedia Earth and Planetary Science 1 (2009) 1152–1157
Procedia Earth and Planetary Science
www.elsevier.com/locate/procedia

The 6th International Conference on Mining Science & Technology

# Derivation of the green vegetation fraction from TM data of three gorges area

Zhang An-bing*, Liu Xin-xia, Di Wei-jin

*School of Resource, Hebei University of Engineering, Handan 056021, China*

**Abstract**

Fraction of green vegetation, $f_g$ is needed as one of regular parameters for vegetation cover analysis. The paper explores the potentials of deriving this variable from thermal mapper (TM) normalized difference vegetation index (NDVI) data considering the leaf area index (LAI) of agricultural field. Geometric, radiometric and atmospheric correction of the images were performed before further analysis. According to the sub-pixel structure characteristic, we choose mosaic-pixel model for calculating percent vegetation cover. A new method was put forward to achieve LAI values of non-dense vegetation where soil line equation was considered. Two schemes are produced to obtain different LAI values and type-specific accuracy is evaluated using parameter defined in this paper.

*Keywords*: leaf area index; fraction of green vegetation; normalized difference vegetation index (NDVI)

## 1. Introduction

The objective of this study is to investigate the method of percent vegetation cover quantification. Firstly, geometric, radiometric and atmospheric correction performance utilized to remotely sensed TM image obtains ground reflectance. Then, we developed simple relationships between actual reflectance in the visible and near infrared band for LAI. At last, the mosaic-pixel model is applied to evaluate percent vegetation cover. Dense model and non-dense model for fraction of green vegetation calculation is used to generate two different results and the standard deviation distribution of the area is given (Sobrino,1990; Gutman,1998; Dymond,1992).

## 2. Study area

The study area approximately 1800 $km^2$ is chosen in the south of Yichang in three gorges area because of the changjiang river and the main changes occurring on the south.


Fig. 1. Location of study area in the middle of China

* Corresponding author. Tel.: +86-13722398191;.
*E-mail address:* liuxinxia999@163.com.


doi:10.1016/j.proeps.2009.09.177

## 3. Image preprocessing

### *3.1. Geometric and radiometric correction*

A geometric correction is necessary for further analysis. The images were geometrically corrected with nearest-neighbour interpolation scheme using ground control points obtained from topographic chart (1:50 000).

The satellite image is handed to the analyst as a set of ditital numbers (DN), consisting of series of bits and ranging from 0 to 255. Sometimes the use of DN-values is satisfactory, but often the values must be converted to radiance of reflectance for futher analysis. The correction procedure including two steps: First, the DN-values were converted into radiance by the following formula (Gillies, 1995; Lambin, 1996).

$$L_\lambda = G_{rescale} \times Q_{cal} + B_{rescale}$$

where: $G_{rescale}$ and $B_{rescale}$ are band-specific rescaling factors typically given in the NLAPS product header file and the product generation work order report.

The final step was to convert the radiance to reflectance by the following equation:

$$\rho_p = \frac{L_\lambda \cdot d^2 \cdot \pi}{ESUN_\lambda \cdot \cos\theta_s}$$

where: $\rho_p$ : Unit less planetary reflectance; $L_\lambda$ : Spectral radiance at the sensor's aperture; d: Earth-Sum distance in astronomical units; $ESUN_\lambda$ : Mean solar exoatmospheric irradiances; $\theta_s$ : Solar zenith angle in degrees; Solar exoatmospheric spectral irradiances $ESUN_\lambda$ for the L5 TM using chance spectrum CHKUR.

### *3.2. Atmospheric correction scheme for the satellite image*

In the study, atmospheric correction of the RED and Near Infrared reflectance band of TM image was carried out using "6S" program (Goddard Space Flight Center, USA ) which was adopted by authors in SUN SPARC workstation. After atmospheric correction the histograms of NDVI were calculated. The comparison of the histogram indicates that the atmospherically corrected NDVI maximum value increase from 0.76 to 0.88 and mean value increase form 0.46 to 0.58.

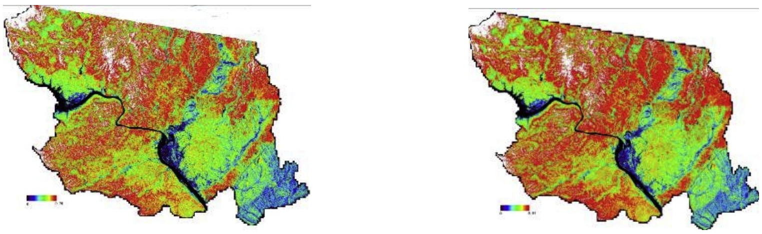

Fig. 2: Comparison of NDVI distribution map before and after using 6S atmospheric correction model. Left panel shows NDVI values ignoring atmospheric effects while right panel shows atmospheric corrected NDVI

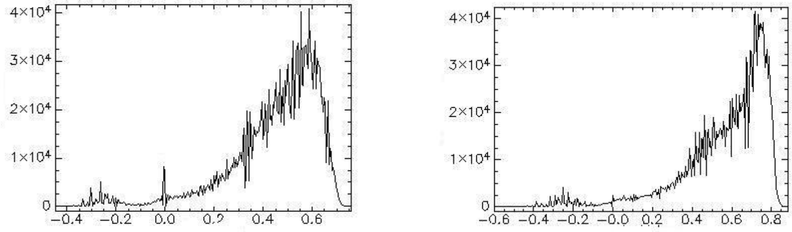


Fig. 3. Comparison of NDVI histogram map before and after using 6S atmospheric correction model. Left panel shows NDVI histogram ignoring atmospheric effects while right panel shows atmospheric corrected NDVI histogram

## 4. Model calculating fraction of vegetation cover

The same NDVI quantity may result from different sub-pixel structures of per unit area of ground. Table 1 shows possible combinations of horizontal and vertical densities and their respective models, which are discussed below (Kerr, 1992).

### *4.1. Uniform-pixel model*

When pixels fully covered by green vegetation ($f$=1) with a certain vertical density, relationship between NDVI and LAI can be described according to Beer's law:

$$NDVI = NDVI_{\infty} - (NDVI_{\infty} - NDVI_0)\exp(-kL_g)$$

where *NDVI* and *NDVI*, are the values from bare soil ($L_g \to 0$) and dense green vegetation ($L_g \to \infty$) respectively, k is the extinction coefficient, and *L* denotes green leaf area index.

### *4.2. Mosaic-pixel models*

If we assumed that a pixel has a mosaic structure, there exists three cases: dense vegetation, nondense vegetation and variable density vegetation (Gillies, 1995; Kerr, 1992). The pixel is not completely covered by vegetation and the NDVI value of a pixel is decided by a weighted average of vegetation cover area and bare area. If we introduce $f_g$ to symbolize green vegetation fraction, then exists:

$$NDVI = f_g NDVI_g + (1 - f_g) NDVI_0 .$$

In the case of dense vegetation, an assumption is made that the density of the vegetated part of the pixel is very high so that:

$$LAI \to \infty, NDVI_g \to NDVI_{\infty} .$$

We can get:

$$f_g = \frac{NDVI - NDVI_0}{NDVI_{\infty} - NDVI_0} .$$

In the case of non-dense vegetation, i.e., $LAI << \infty$, $f_g$ is calculated by:

$$f_g = \frac{NDVI - NDVI_0}{NDVI_g - NDVI_0} ,$$

$$NDVI_g = NDVI_{\infty} - (NDVI_{\infty} - NDVI_0)\exp(-kL_g) .$$

In reality, there exists several vegetation types within a pixel, and their vertical densities may vary, so that the observed NDVI, is a weighted average of the NDVIs from different vegetated 'tiles' of the vegetated ($NDVI_{gi}$) and non-vegetated ($NDVI_0$) parts.

$$NDVI = \sum f_{gi} NDVI_{gi} + (1 - \sum f_{gi}) NDVI_0$$

$$NDVI_{gi} = NDVI_{\infty} - (NDVI_{\infty} - NDVI_0)\exp(-k_i L_{gi})$$

Table 1. The schematic representation of sub-pixel models for vegetation fraction

| Pixel type | Mosaic-pixel model | Figure | Formula |
|---|---|---|---|
| Uniform-pixel model | Fully covered vegetation |  | $f_g = 1$,NDVI is determined by LAI |
| Mosaic-pixel model | Dense vegetation | 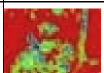 | $f_g = \frac{NDVI - NDVI_0}{NDVI_{\infty} - NDVI_0}$ |
| | Nondense vegetation | 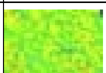 | $f_g = \frac{NDVI - NDVI_0}{NDVI_g - NDVI_0}$ |
| | Variable density vegetation | 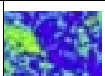 | $NDVI = \sum f_{gi} NDVI_{gi} + (1 - \sum f_{gi}) NDVI_0$ |

### *4.3. Choosing an appropriate mosaic-pixel model for TM image*

Jointly consideration of the spatial resolution of satellite sensor data and the structure of vegetation can be used for choosing appropriate pixel. The mosaic-pixel model is applied to TM image for fraction of vegetation.

## 5. Estimating LAI from radiometric correction TM image

### *5.1. Theory background on LAI estimation*

We consider a vegetation canopy having a leaf area index (LAI) above a soil of reflectance $r_s(\lambda)$, where $\lambda$ is the wavelength. The reflectance above the soil and canopy is given by (Quamby,1992):

$$R(\lambda) = \left[ r_\infty + \frac{D}{r_\infty} \right] \Big/ (1 + D) \tag{1}$$

where

$$D = \frac{r_s - r_\infty}{(1/r_\infty) - r_s} \cdot e^{-2c \cdot LAI} \tag{2}$$

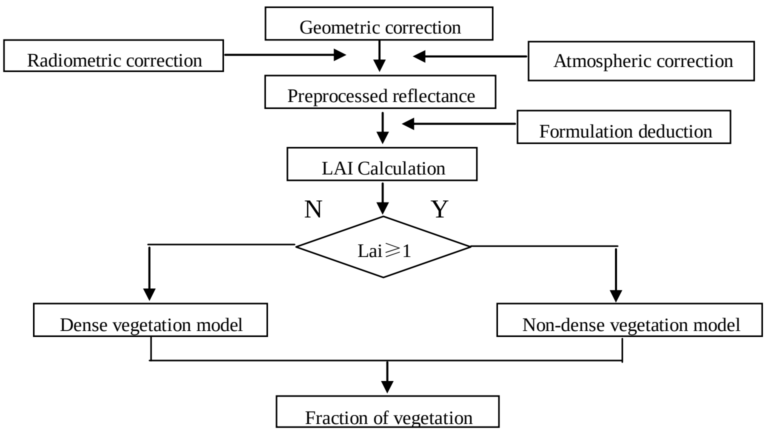


Fig. 4. Estimation of fraction of vegetation

Fig.4. shows the Estimation methodology of LAI value associated with nondense vegetation model is described in section 5. Which was used by Price (Price, 1987) previously for retrieval of LAI. $r_\infty$ denotes the reflectance of dense canopy (LAI=$\infty$), c describe the attenuation of radiation as it passes through successive layers of leaves. Then, considering equation (1) and (2), we find:

$$r_{si} = \frac{R_i(r_{\infty i}^2 - e^{2c_i LAI}) + r_{\infty i}(e^{2c_i LAI} - 1)}{R_i r_{\infty i}(1 - e^{2c_i LAI}) + r_{\infty i}^2 e^{2c_i LAI} - 1} \tag{3}$$

Where, subscript *i*(=1, 2) represent visible and near infrared wavelengths respectively. plus the equation of the soil line:

$$r_{s2} = a \cdot r_{s1} + b \tag{4}$$

LAI may be obtained as a function of the actual reflectances above the canopy, $R_1$ and $R_2$ approximately equal to corrected reflectances from TM image. Solution of LAI also requires knowledge of a number of constants:

(1) The soil line constants, a and b, are required. In this research, the soil line was obtained from a scattergram of remotely sensed data.

(2) $C_1$, $C_2$ are given 0.6 and 0.21 respectively depending on experimental results of Price associated with agricultural area and grass land. $r_{\infty 1}$ and $r_{\infty 2}$ were set to 0.05 and 0.7 according to Price also.

### *5.2. Experimental result of LAI estimation*

For this study an typical area of the region was selected, the scattergram representing the scatter points distribution between visible and near-infrared band is shown in Fig.5. The soil line of the specific vegetation cover area also is shown. linear regression was used to generate slope and intercept values relating to Red and NIR reflectance space of the soil line. Here the regression equation is (Carlson, 1997):

$$r_{s2} = 1.0033 r_{s1} + 0.0099675 \tag{5}$$

Contour was constructed for spaced points in the range R1(0-0.4), R2(0-0.6). LAI value corresponding to visible and near infrared band reflectance value can be obtained from the figure.

## 6. Experiment and result analysis

### *6.1. Interpretation TM image for using mosaic models*

Probing to different vegetation cover type, we perform model-oriented interpretation. Eight types and the corresponding percent vegetation cover calculation model is shown in Table.1. Result is shown on Fig.6 show the distribution of different.

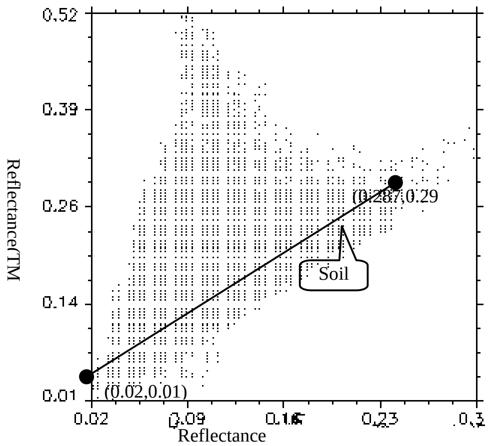


Fig. 5. A scattergram is shown for data from a Thematic Mapper image of a typical agricultural area in YICHANG. The abscissa corresponds to visible band data, the ordinate to near infrared band

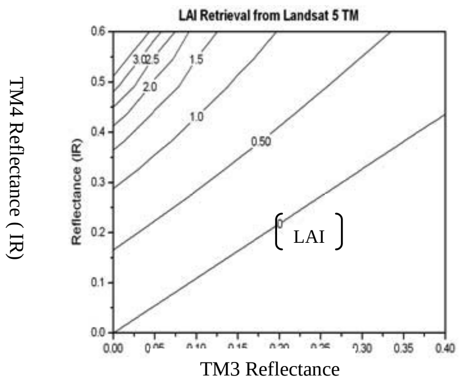


Fig. 6. This figure illustrates derived values of LAI as a function of Landsat digital counts, for the parameters given in the text. Contour lines correspond to constant values of LAI

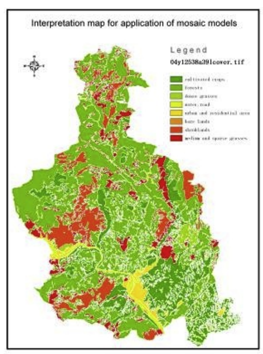


Fig. 7. Interpretation map for application of mosaic models from TM image of 2004

Table 2. Percentage of Interpretation map for application of mosaic models from TM image of 2004

| Cover type | Cultivated crops (%) | Forest (%) | Dense grasses (%) | Medium andsparse grasses (%) | Water area and load (%) | Urban and residential area (%) | Bare lands (%) | Shrublands (%) |
|---|---|---|---|---|---|---|---|---|
| Of total | 28.8 | 41.4 | 1.8 | 6.7 | 7.2 | 3.0 | 0.2 | 10.9 |

| | | | | | | | | |
|---|---|---|---|---|---|---|---|---|
| Chosen model | Nondense model | Dense model | Dense model | Constant 0 | Dense model | Constant 0 | Nondense model | Nondense model |

*6.2. Calculation result of fraction of green vegetation*

Percent vegetation cover resulting from dense and nondense model are calculated respectively, $NDVI_0$ and $NDVI_\infty$ values are obtained directly reading from corrected TM image.

*6.3. Evaluation of differences of the two methods*

Simulating to standard deviation definition, we give statistic defined as:

$$s = \sqrt{\frac{1}{n}\sum_{i=1}^{n}(x_i - y_i)^2} \tag{6}$$

Where, $x_i, y_i$ denote fraction green vegetation value calculated by dense and nondense model respectively, n is pixel count of the corresponding cover type.

The statistic residual value of different vegetation cover type is compared in Table 2

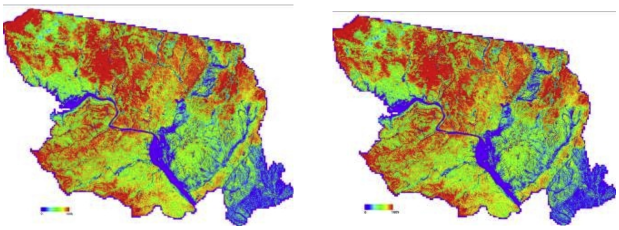

Fig. 8. LAI value distribution map (Left: Dense model; Right: Nondense)

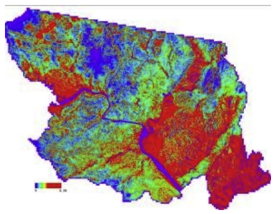

Fig. 9. The differences of dense model and nondense model

Table 3. Deviation of different model-oriented vegetation type

| Cover type | Cultivated crops | Forest | Dense grasses | Water area and road | Urban and residential area | Bare lands | Shrublands | Medium and sparse grasses |
|---|---|---|---|---|---|---|---|---|
| deviation | 0.14186 | 0.072737 | 0.11704 | 0 | 0.25708 | 0 | 0.088138 | 0.10271 |

## Acknowledgements

This paper is supported by the Specialized Research Fund for the Doctoral Program of Higher Education of China (200802901516, 200802900501) and in part by China-Australia Special Fund for Scientific and Technological Cooperation (50810076).

## References

[1] J.A. Sobrino, V. Caselles and F. Becker, Significance of the Remotely Sensed Thermal Infrared Measurements Obtained Over a Citrus Orchard. Photogrammetric Engineering and Remote Sensing. 44 (1990) 343-354.

[2] G. Gutman and A Ignatov, The Derivation of the Green Vegetation Fraction from NOAA/AVHRR Data for Use in Nurderical Weather Prediction Models. International Journal of Remote Sensing. 19 (1998) 1533-1543.

[3] J.R. Dymond, P.R. Stephens and P.F. Newsome, Percent Vegetation Cover of a Degrading Rangeland from SPOT. International Journal of Remote Sensing, 13 (1992) 1999-2007.

[4] R.R. Gillies and T.N. Carlson, Thermal remote sensing of surface soil water content with partial vegetation cover for incorporation into climate models. Journal of Applied Meteorology. 34 (1995) 745-756.

[5] E.F. Lambin and D. Ehrlich, The Surface Temperature Vegetation Index Space for Land Cover and Land cover Change Analysis. International Journal of Remote Sensing. 17 (1996) 463-487.

[6] Y.H. Kerr, J.P. Lagouarde and J. Imbernon. Accurate land surface temperature retrieval from AVHRR data with use of an improved split-window algorithm. Remote Sensing of Environment. 46 (1992) 319-330.

[7] N.A. Quamby, J.R.G. Townshend and J.J. Settle, Linear Mixture Modeling Applied to AHVRR Data for Erop Area Estimation. International Journal of Remote Sensing. 13 (1992) 415-425.

[8] C.J. Price, Calibration of Satellite Radiometers and the Comparison of Vegetation Indices. Remote Sensing of Environment. 21 (1987) 15-27.

[9] T.N. Carlson and D.A. Ripley. On the Relation Between NDVI, Fractional Vegetation Cover, and Leaf Area Index. Remote Sensing of Environment. 62 (1997) 241-252.